Quarterly Journal of the Royal Meteorological Society *Q. J. R. Meteorol. Soc.* 140: 2197–2210, October 2014 A DOI:10.1002/qj.2289

RMetS
Royal Meteorological Society

Seasonal dependence of the urban heat island on the street canyon aspect ratio

N. E. Theeuwes,* G. J. Steeneveld, R. J. Ronda, B. G. Heusinkveld, L. W. A. van Hove and A. A. M. Holtslag

Meteorology and Air Quality Section, Wageningen University, The Netherlands

*Correspondence to: N. Theeuwes, Meteorology and Air Quality Section, Wageningen University, PO Box 47, 6700 AA, Wageningen, The Netherlands. E-mail: natalie.theeuwes@wur.nl

In this article we study the relation between the urban heat island (UHI) in the urban canyon and street geometry, in particular the aspect ratio. Model results and observations show that two counteracting processes govern the relation between the nocturnal UHI and the building aspect ratio: i.e. trapping of long-wave radiation and shadowing effects. In general, trapping of long-wave radiation supports the UHI, whereas shadowing effects reduce the UHI. The net effect depends on the UHI definition and the amount of available short-wave radiation penetrating the canyon. In summer, autumn and spring the shadowing effects can already reduce the UHI starting at an aspect ratio between 0.5 and 1. The analysis is carried out using several methods. Firstly, the single-column model version of the Weather Research and Forecasting (WRF) model is used extensively. Two separate runs, one rural and one urban, are used to estimate the UHI. Secondly, the urban canyon temperature at the 2 m level is introduced, which allows for direct comparison between modelled and observed air temperatures within the urban canyon. Finally, the model is evaluated for all four seasons. The results of this research provide important insights for urban planning on how to use the aspect ratio to mitigate the UHI in the urban canyon.

Key Words: urban heat island; urban morphology; radiative trapping; street geometry; WRF; urban meteorology; canyon temperature; The Netherlands

Received 20 December 2012; Revised 30 August 2013; Accepted 30 October 2013; Published online in Wiley Online Library 12 February 2014

1. Introduction

Presently, most of the world population resides in urban areas. Cities are expanding fast in many parts of the world (United Nations, 2006). The enhanced urbanisation is expected to further increase the urban heat island (UHI) effect (the difference between the urban and rural air temperature), which is already substantial in numerous cities around the globe (e.g. Kim and Baik, 2005; Hidalgo *et al.*, 2008; Steeneveld *et al.*, 2011). Taking into account the projected increase in frequency and intensity of periods of extreme heat due to climate change (Solomon *et al.*, 2007; Fischer and Schär, 2010), urbanisation may pose serious challenges for cities regarding human thermal comfort and health (e.g. Kovats and Hajat, 2008; McCarthy *et al.*, 2010).

The spatial planning of urban areas provides the opportunity to mitigate these adverse effects of urbanisation and climate change in order to create a more comfortable urban living environment. However, implementing mitigation measures requires a better understanding of urban environmental physics, in particular the effect of urban morphology on urban environmental physics (e.g. Lenzhölzer and Van der Wulp 2010).

Urban morphology is characterised by factors such as the way buildings and streets are configured, building properties, etc. In order to quantify the building density or street set-up, the sky-view factor and aspect ratio are widely used indicators. The sky-view factor is defined as the fraction of sky that can be seen from a certain point in the street canyon. The aspect ratio is the height of the buildings divided by the width of the street. In areas with a high building density, the sky-view factor is usually low, while the aspect ratio is high.

Relations between the UHI magnitude and street geometry were first examined by Oke (1981, 1988). Using observations and a relatively simple model, a clear positive logarithmic relation was found between the aspect ratio and the year-round maximum canopy layer UHI. Oke *et al.* (1991) reproduced these results with a model. However, this model did not include short-wave radiation and turbulence, and had a constant value for long-wave downwelling radiation. In addition, Giannopoulou *et al.* (2010) performed measurements in three streets with different street geometries and found a decrease of the diurnal temperature range and cooling rate with an increased aspect ratio.

Recent studies have used urban canopy models to determine the relation between street geometry and the urban energy budget. Marciotto *et al.* (2010) for instance used a simple urban canopy model, similar to the one used in this study, to estimate the urban canyon temperature for São Paulo, Brazil. Surprisingly, they found a maximum in the nocturnal temperature at an aspect ratio of around 3.5. For very high aspect ratios (>3.5), increasing

© 2013 Royal Meteorological Society

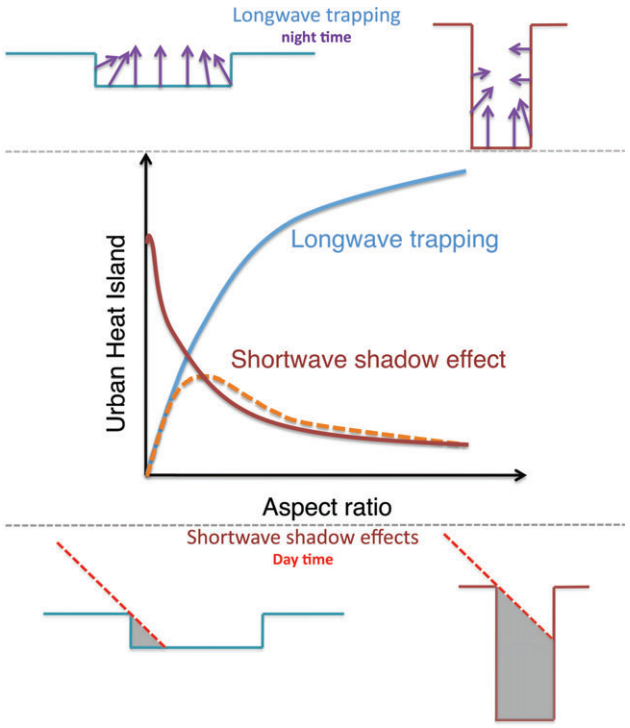

Figure 1. A schematic drawing of the two processes involved in determining the relationship between the canyon heat island and the aspect ratio.

the aspect ratio led to a *lower* nocturnal temperature rather than a higher temperature as expected from the extrapolation of the Oke (1981, 1988) results. This maximum raises the question of which additional process is responsible for this behaviour.

The goal of this research is to examine the different processes involved in regulating the influence the aspect ratio has on the street level UHI (at 2 m above the surface) for different seasons in midlatitudes. We attempt to explain the contradictions in previous studies by studying the processes using a single-column model, an approach similar to Hamdi and Schayes (2008). This experiment was first performed for a case with idealized thermodynamic profiles and a 12 h day and night. Next, four different realistic cases in the different seasons are examined for the midlatitude city of Rotterdam (The Netherlands).

One of the novel aspects of this study is the validation of the model results with UHI observations at various sites in the second largest city in the Netherlands, i.e. Rotterdam. A robust way to reach the main research goal is through this combination of model results and observations.

In the next section, the basic concepts tested in this study will be hypothesized. In section 3, a model description is given. In section 4, an idealized case-study will be described and used to examine the processes involved in determining the influence of street geometry on the UHI. This theory will be applied to four real cases for different seasons in section 5. Finally, the conclusions are drawn in section 6.

2. Concepts

In this section the processes influencing the relation between the street canyon aspect ratio and the UHI will be described. However, first we establish our definition of the UHI. Here, the UHI is defined as the difference in air temperature at 2 m in the urban canyon and in the rural environment. Considering the temporal aspect of the UHI, we use the UHI during the night in two different definitions. First, we label the UHI in the evening from section 4.2 the maximum UHI:

$$UHI_{\max} = \max(T_{\text{urban}} - T_{\text{rural}}). \tag{1}$$

This UHI definition is mainly used in literature (e.g. Oke, 1981, 1988; Chow and Roth, 2006; Steeneveld *et al.*, 2011). The second definition represents how much the city eventually cools compared to the rural area and is represented by the difference in minimum temperature between the urban and rural environment ($UHI_{T\min}$) (also used by Gallo *et al.*, 1993; Houet and Pigeon, 2011):

$$UHI_{T\min} = \min(T_{\text{urban}}) - \min(T_{\text{rural}}). \tag{2}$$

In the idealized cases in this study, the minimum temperature occurs at the end of the night, and is approximately simultaneous for the urban and rural area. In other cases (different weather or location), this may not be the case. Both definitions will be used in the remainder of this study.

Concerning the relation between $UHI_{\max}$ and the building aspect ratio, previous research raised some questions. Oke (1981, 1988) and Hamdi and Schayes (2008) found a clear positive correlation between the aspect ratio and $UHI_{\max}$, whereas Marciotto *et al.* (2010) report a maximum in the relationship between the nocturnal temperature at an aspect ratio of about 3.5. This is followed by a decrease in the nocturnal temperature with an increasing aspect ratio.

The results of these studies can be conceptually explained by the presence of two counteracting processes. First, because of *trapping of long-wave radiation*, heat is kept inside the urban canyon if the buildings become higher and the street width smaller. Thus, the trapped energy warms the canyon and consequently the UHI increases (Figure 1). The other mechanism is the *shadowing effect*, which inhibits the warming of the canyon. Narrow streets and high buildings have a larger shaded area in the urban canyon. Therefore, a higher aspect ratio leads to a lower temperature during the day. Due to the relatively high thermal inertia of the urban canopy system, a lower temperature during the day will also cause a relatively lower temperature during the night. Therefore, a higher aspect ratio leads to a lower UHI (Figure 1).

We hypothesize that the combined effect of the two processes will result in an optimum UHI for a specific aspect ratio. This means, from a certain aspect ratio, shadowing effects start to become more important than the trapping of long-wave radiation effect for the UHI.

3. Model description

We combine model results and field observations to determine the relationship between the UHI and street geometry. The weather research and forecasting model (WRF) version 3.4.1 (Skamarock *et al.*, 2008) is employed.

The WRF model is used in single-column mode and includes the single-layer urban canopy model (SLUCM; Kusaka *et al.*, 2001; Chen *et al.*, 2011). Several versions of the SLUCM participated in the PILPS*-urban international comparison of urban energy balance models (Grimmond *et al.*, 2010, 2011). Within this intercomparison, the WRF implementation of the model performed relatively well for above-canyon fluxes (i.e. in the first quantile for net radiation, sensible and storage heat fluxes).

The SLUCM in WRF is combined with the Noah land surface scheme (Ek *et al.*, 2003). SLUCM has a single model layer for the urban component and uses a tile approach to include vegetation within the urban area. This means that the energy balance is calculated separately for the vegetated and the impervious surfaces. The resulting energy balance components, upward short-wave and upward long-wave radiation, are subsequently fed back to the atmospheric model. The focus of our research is on street geometry. Therefore, the areal surface vegetation cover is set to a fixed fraction. For the impervious part, the SLUCM considers radiative trapping, shadow effects and single reflection on the facades (explained in the Appendix). The estimation of the

*PILPS: Project for Intercomparison of Land-surface Parametrization Schemes.

© 2013 Royal Meteorological Society

radiation components is not as complex as in a multi-layer canopy model, but is sufficient for representing the concepts presented in section 2.

The canyon vertical heat flux follows from solving the surface energy balance for the road and walls. The scheme uses a resistance approach to describe the turbulent transport between the lowest model layer and the urban canopy and within the canyon itself. Within this approach, the wind speed and atmospheric stability control the turbulent transfer. For the calculation of the canyon wind speed, we refer to the Appendix. Furthermore, the anthropogenic heat is assumed to be zero in all cases, because only the effect of the aspect ratio will be analysed. It is likely that a higher aspect ratio would lead to more anthropogenic heat, due to the increased human activity that could take place in higher buildings. However, this will not be taken into account in this study since the quantitative relation between aspect ratio and anthropogenic heat is uncertain and will differ between cities. On the other hand, anthropogenic heat is indirectly included in the model by means of keeping the indoor temperature constant.

Ideally, we wish to evaluate the model with observations taken in the canyon. The standard canyon temperature in SLUCM is calculated from the surface temperatures of the road and the walls, the canyon wind speed, the lowest model-level temperature, and the roughness length for heat (in the default case, 0.137 m). This canyon temperature acts as an effective skin temperature of the urban canyon. Preliminary model experiments using the canyon temperature show a typical clear sky summer day in midlatitudes has a diurnal temperature range of more than 20 K and a maximum temperature of 47 °C. No observations within the urban canyon of Dutch cities support these high values (Heusinkveld *et al.*, 2013). Consequently, we revised the estimation for the modelled canyon temperature in order to ensure a meaningful comparison to measurements in the urban canopy.

The revision consists of the following modification. In the original scheme, the stability correction was applied between the atmospheric model and the roughness length for heat, rather than to the 2 m level. In the revised scheme, the canyon temperature is based only on the sensible heat flux originating from the urban canyon (the wall and road sensible heat flux combined), and the stability correction is applied to the 2 m level. Here, for simplicity a standard logarithmic temperature profile is assumed with stability corrections using Monin–Obukhov similarity theory:

$$T_{2\mathrm{m,canyon}} = T_\mathrm{a} + \frac{H_\mathrm{C}\, r_\mathrm{ah}}{\rho C_p}, \tag{3}$$

$$r_\mathrm{ah} = \frac{1}{\kappa u_*}\left\{\ln\left(\frac{z_\mathrm{a}}{z_\mathrm{2m}}\right) - \Psi_\mathrm{h}\left(\frac{z_\mathrm{a}}{L}\right) + \Psi_\mathrm{h}\left(\frac{z_\mathrm{2m}}{L}\right)\right\}, \tag{4}$$

and the Obukhov length (L) is

$$L = -\frac{\rho C_p T_\mathrm{a} u_*^3}{\kappa g H_\mathrm{C}}. \tag{5}$$

The stability functions are:

$$\Psi_\mathrm{h}\left(\frac{z}{L}\right) = \begin{cases} 2\ln\left\{\dfrac{1+\left(1-16\dfrac{z}{L}\right)^{\frac{1}{2}}}{2}\right\} & \text{for } \dfrac{z}{L} < 0, \\ -5\dfrac{z}{L} & \text{for } \dfrac{z}{L} \geq 0. \end{cases} \tag{6}$$

In Eq. (3), T_a is the air temperature of the lowest model level above the urban canyon, H_C is the sensible heat flux from the canyon, ρ is the air density, C_p is the specific heat capacity of dry air, u_* is the friction velocity of the urban canopy (roof and canyon combined) calculated using similarity stability functions, κ is the von Kármán constant (= 0.4) as in Högström (1996) and g is the acceleration of gravity (=9.81 m s^{-2}), and z_a and z_2m are the height of the lowest atmospheric model level (in this case 26 m) and 2 m, respectively. How the resulting temperature compares to observations is presented later in this study.

The WRF 1D model is run with 60 vertical levels, with the lowest model level at 26 m and with a time step of 30 s. The boundary conditions (geostrophic wind, subsidence, temperature, moisture and momentum advection) can be prescribed in the model at any chosen time (interval). In this study, only the geostrophic wind speed is prescribed. In addition, within our set-up the Yonsei University (YSU) boundary-layer scheme (Hong *et al.*, 2006) is used, because a non-local scheme has the least cold bias at night in the urban (Pino *et al.*, 2004) and rural boundary layer (Hu *et al.*, 2010). The Mellor–Yamada–Janjic and Quasi-Normal Scale Elimination boundary-layer schemes were also tested. However, both gave insufficient mixing during the night in a rural environment during winter, leading to the temperature during the night being much lower than observed.

For completeness, the relatively simple microphysics scheme from Lin *et al.* (1983) is used, because only cloudless cases were selected. As for the radiation, the Rapid Radiative Transfer Model (RRTM) (Mlawer *et al.*, 1997) is used for the long-wave radiation. We used the relatively simple Dudhia (1989) scheme for the short-wave radiation, because aerosols or clouds are not considered.

4. 'Idealized' case

This study consists of two sets of experiments. The first, an 'idealized' case, examines the processes described in section 2. The idealized case provides an appropriate set-up for the research objective, which is to determine the processes involved in the influence of the aspect ratio on the UHI. The second, consisting of four 'real' cases, aims to identify the importance of each process in the four different seasons. This section describes the case set-up and the results of the 'idealized' case. The results are evaluated in three steps. First, the results of the modelled idealized case are described. Second, this case will be used to examine the relationship between the UHI and street geometry. Finally, the sensitivity of the results is evaluated with respect to the geostrophic wind speed and several model parameters.

4.1. *Case set-up*

The single-column model version of WRF is used to perform multiple fast runs in a fully controllable, idealized set-up. This approach is advantageous because it avoids the impact of large-scale phenomena, while external forcings can be controlled. Since the results cannot be related to city size or horizontal resolution of the model, results solely depend on the aspect ratio.

The term 'idealized' is used because idealized initial profiles and large-scale forcings are used to run the model, i.e. there are no clouds or residuals of large-scale or mesoscale phenomena in the profiles. The case is initialised at 1200 UTC, i.e. 1 h after solar noon and is run at a latitude of 51°N (The Netherlands) for 24 h in March – a 12 h day and 12 h night. The mean boundary-layer potential temperature (Θ) and specific humidity (q) are about 293 K and 5.7 g kg^{-1} with a Θ and q jump of about 4 K and −3 g kg^{-1} respectively at 1.9 km above sea level. These values are based on observations of the Cabauw tower (Beljaars and Bosveld, 1997) on 7–10 May 2008. During this time, an anticyclone was centred to the north of the Netherlands and no fronts were in the vicinity. The wind speed is assumed to be constant and equal to the geostrophic wind speed above 1 km at 3 m s^{-1} while below 1 km a logarithmic wind profile is adopted using the local friction velocity. For the rural and urban environment, the background surface albedos amount to 0.23 and 0.20 (for each of the three facades), the roughness length 0.15 and 0.33 m (urban canopy) and the surface emissivity 0.99 and 0.90 (for each of the three facades), respectively. In order to keep the

© 2013 Royal Meteorological Society

Bowen ratio of the grassland simulation about 0.3 during the day, as was observed, the soil temperature at a depth of 0.7 m is 284 K and the volumetric soil moisture fraction is 0.387 in both cases. Finally, advection of any kind (large- or small-scale, moisture, temperature or momentum) is neglected in the single-column model simulations to keep the case idealized.

Using the described set-up, we estimate the UHI by separately simulating two surfaces, one for a grassland (Noah) and another for an urban surface (Noah coupled to SLUCM). The street canyon aspect ratio ranges from 0 to 6.7 within the city of Rotterdam, The Netherlands, with an average of about 1 in the city centre. Therefore, the default aspect ratio is 1 (road width of 14 m and building height of 14 m). The roof width is 10 m, the wall thickness is 40 cm and indoor temperature is assumed to be 17 °C. The other urban parameters are set as in Chen *et al.* (2011).

4.2. *Case results*

The 2 m air temperature in the urban environment is found always to be higher than that of the grassland environment (Figure 2(a)), implying the UHI is always positive in this case (Figure 2(b)). The UHI is largest in the early evening, amounting to about 6 K, approximately similar to the 95 percentile of the UHI_{max} in several Dutch cities found by Steeneveld *et al.* (2011). During the day the UHI has a minimum of 2 K. Throughout the night the UHI decreases by about 2 K. This is the difference between UHI_{max} and UHI_{Tmin}.

Figure 2(c) shows that the grassland environment starts to cool slightly earlier and at a much faster rate than the urban environment. After the sun sets, it takes more time for the still unstable layer above the urban area to cool down. This is partly caused by the difference in thermal properties of pervious and impervious surfaces. Moreover, the cooling rate is lower due to the heat still contained in the system after the large uptake of heat by the urban fabric during the day (Figure 2(d)). During the night both the urban and rural environment show similar behaviour and cool until sunrise at 0600 local time (LT). After sunrise the grassland appears to heat up faster than the urban environment. However, the difference in the heating rate magnitude is smaller than the difference in the cooling rate in the evening. Therefore, it is concluded that the difference in cooling rate, rather than the heating rate, mainly contributes to the formation of the UHI, a conclusion in agreement with Oke (1982).

The urban energy balance is displayed in Figure 2(d). The sensible heat flux in the urban canyon is slightly larger than above a rural surface and shows a small delay compared to the rural sensible heat flux. As a result of the absence of anthropogenic heat, the sensible heat flux becomes slightly negative during the night. The storage heat flux in the canyon is much larger and the maximum is earlier than the sensible heat flux. This is consistent with previous studies (Oke *et al.*, 1999; Masson *et al.*,

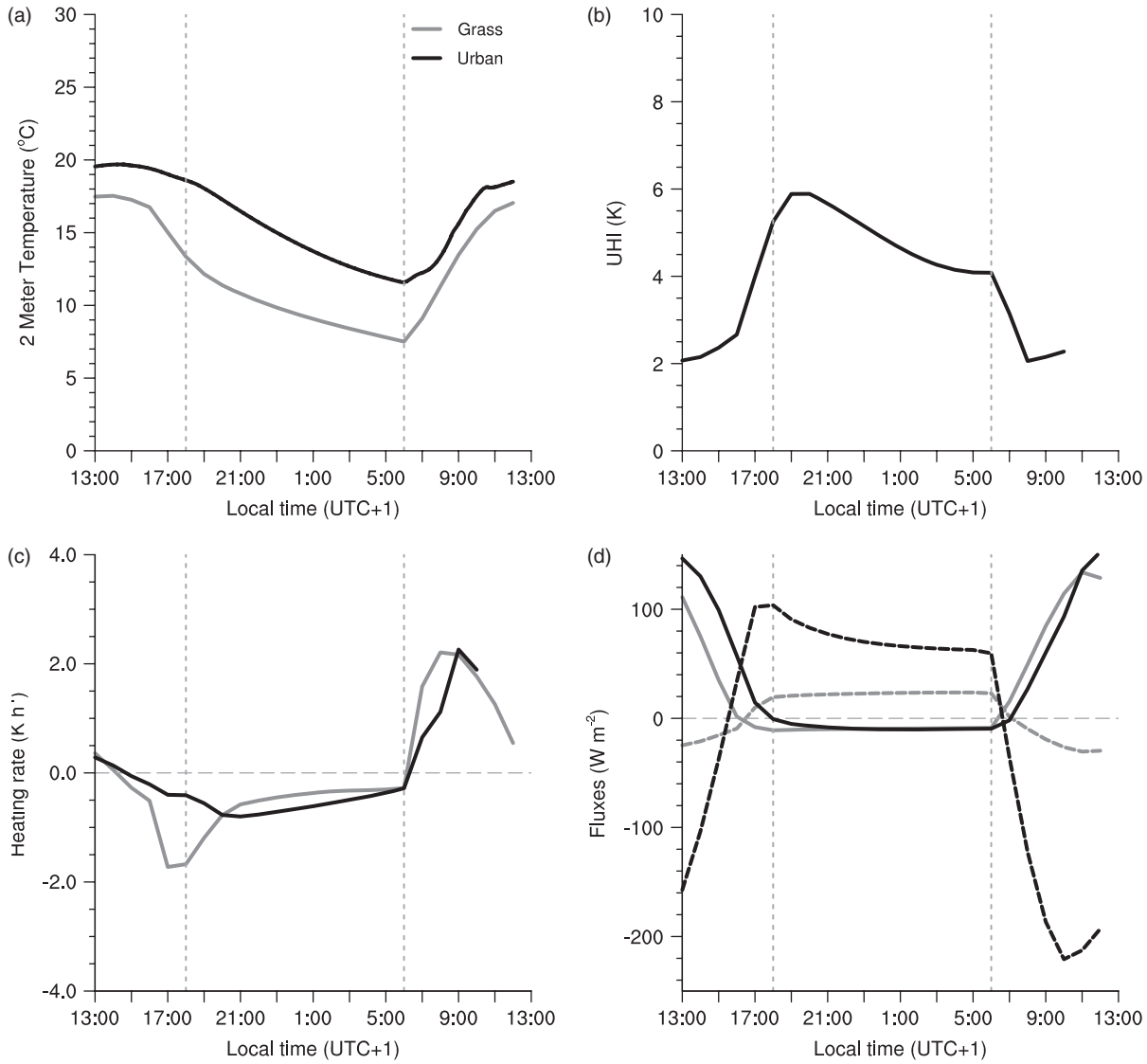

Figure 2. The modelled (a) 2 m temperature, (b) urban heat island, (c) heating/cooling rates ($K\,h^{-1}$) of the 2 m air temperature and (d) the canyon sensible (full lines) and ground/canyon storage (dashed lines) heat flux ($W\,m^{-2}$) in the urban canyon (black) and over grass (grey) simulations. The vertical dotted lines denote sunrise and sunset. The model spin-up time is 48 h, the geostrophic wind speed is $3\,m\,s^{-1}$ and the aspect ratio is 1.

© 2013 Royal Meteorological Society

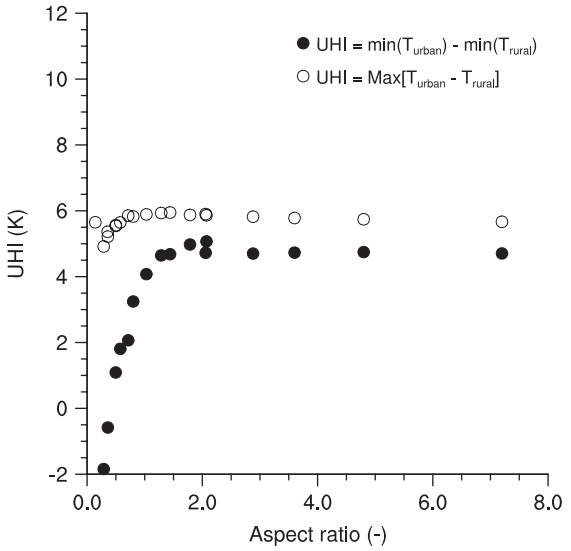

Figure 3. Two definitions of the urban heat island for different aspect ratios: UHI_{Tmin} (solid) and UHI_{max} (open). The model spin-up time is 48 h.

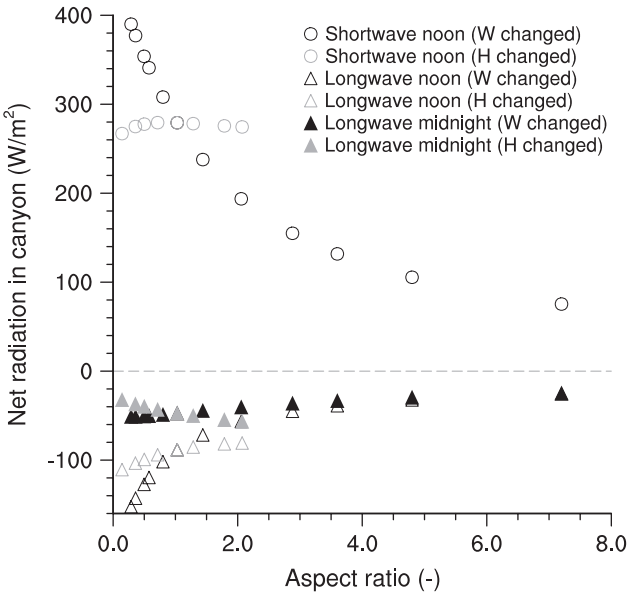

Figure 4. The net short-wave (circles) and long-wave (triangles) radiation within the urban canyon at noon (open symbols) and midnight (solid symbols) for different aspect ratios. When the road width (W) is changed, the symbols are black and a changed building height (H) is indicated by grey symbols. The model spin-up time is 48 h.

2002; Pearlmutter *et al.*, 2005). These two simulations (urban and rural) are used as the default below.

4.3. UHI and the aspect ratio

The aspect ratio can be modified either by changing the building height or the street width. Therefore, the aspect ratio is not a unique parameter (explained later in this section). However, varying both the height of the roof and the width of the street is still a good indicator of the street canyon shape. In the simulations both the building height (from 2 to 29 m) and the street width (from 2 to 50 m) were modified; the aspect ratio ranges from 0.14 to 7.2. This range is larger than found in most cities. However, in order to have a complete picture of the processes involved this larger range is used.

Figure 3 shows the model results for the two definitions of the UHI for different aspect ratios (UHI_{max} and UHI_{Tmin}). The UHI_{Tmin} shows an increase with the aspect ratio until it becomes constant after an aspect ratio of about 2. The negative values of UHI_{Tmin} for very small aspect ratios are caused by the difference in surface properties between the urban and rural environment and the walls are too small to have an influence on the temperature. In the relation between the UHI_{max} and the aspect ratio, the aspect ratio has a positive effect on the UHI until an aspect ratio of about 1 where the effect becomes constant and later even slightly negative.

The explanation for this behaviour lies in the timing of both definitions of the UHI. The UHI_{max} usually takes place during the early part of the night (Figure 2). This is in contrast to the minimum temperature which is reached at the end of the night. A decrease in the street width (increase in aspect ratio) leads to a decrease in the incoming solar radiation (Figure 4). This leads to a decrease in the temperature during the day. Note that this lower temperature is reflected in the early night when the maximum UHI is obtained. This effect is called the shadowing effect. However, this evens out during the night and, at the time the minimum temperature occurs, it no longer plays a role.

For an aspect ratio below 1, the relationship between the aspect ratio and the UHI is straightforward in the model results: increasing the aspect ratio leads to an increased UHI for both definitions. Trapping of long-wave radiation (section 2) causes energy to be stored in the canyon as buildings become higher and streets more narrow. In general, UHI_{Tmin} becomes very small for wide streets and low buildings. This means that a flat concrete (or asphalt, etc.) surface (the aspect ratio approaches zero) is eventually able to reach below the grassland air temperature. However, an aspect ratio approaching zero does not lead to near-zero UHI_{max} values. There is always a difference between the urban and rural simulation, with a minimum of 4.5 K. This is due to the time lag and different magnitudes of the cooling rates (Figure 2).

When the aspect ratio exceeds about 1.5, the situation becomes more complex. The uniform behaviour of the aspect ratio parameter in relation to the UHI is no longer valid. This effect is especially noticeable for UHI_{Tmin}, at an aspect ratio of 2. Increasing the building height has a larger effect on the UHI_{Tmin} than changing the width of the street for the same aspect ratio. This effect is attributed to the model's treatment of the street width as a fraction of the total urban area width (roof width + street width). When the roof width is kept constant, increasing the street width effectively changes the building plan area fraction. This allows relatively more short-wave radiation to be incident into the urban canyon and less to the roof surfaces, with results on the energy balance as well (Harman and Belcher, 2006). Simulations changing the roof width with the street width, keeping the fraction canyon the same, were also performed. These simulations had the same result (for radiation and temperature) as changing the height of the building.

The net short-wave and long-wave radiation in the urban canyon for different aspect ratios are displayed in Figure 4. A decreased street width leads to a decrease in net short-wave radiation from 400 to about 80 W m^{-2}. Since the albedo of the walls and road remains constant, this change can only be explained by a change in incoming short-wave radiation. However, in contrast, changing the height of the roof does not change the net short-wave radiation significantly which remains around 280 W m^{-2}. Therefore, when the aspect ratio reaches values higher than 1, the short-wave radiation entering the urban canyon is higher when increasing the building height than when reducing the street width; this results in a higher UHI_{Tmin} (Figure 3).

This difference between changing the street width and roof height is much less in case of the net long-wave radiation trapped during the night (Figure 4). During the night, increasing the building height will have an increased cooling effect compared to changing the street width, due to the larger wall surface and thus greater outgoing radiation. If the street width is decreased (increasing the aspect ratio, not correcting for the building area index), decreased radiation exits the urban canyon. Thus, the relative contribution to the cooling effect decreases and more

© 2013 Royal Meteorological Society

heat can be trapped in the urban canyon. However, with an aspect ratio larger than 1, changing the height of the buildings or the width of the streets, the difference in net long-wave radiation (L^*) ($L^*_{\mathrm{Hchanged}} - L^*_{\mathrm{Wchanged}}$) (maximum 20 W m^{-2}) is smaller than the difference in net short-wave radiation (S^*) ($S^*_{\mathrm{Hchanged}} - S^*_{\mathrm{Wchanged}}$) (maximum 100 W m^{-2}). Therefore, the above described short-wave radiation effect dominates and causes the UHI to be higher when changing the building height to an aspect ratio of higher than 1 in Figure 3.

Summarizing, there are two counteracting processes governing the relationship between the UHI and the aspect ratio, as explained in section 2. Trapping of long-wave radiation limits the cooling of a street canyon during the night when buildings are high and streets are narrow. Thus, trapping of long-wave radiation leads to an increase in the UHI during the night. On the other hand, the shadowing effect limits the amount of radiation reaching into the canopy for a large aspect ratio. This effect leads to a decrease in the UHI for large aspect ratios. These two processes can guide city planners on how to use the aspect ratio in designing to create more comfortable environments. For example, higher buildings or more narrow streets do not necessarily imply higher temperatures. In addition, the difference in changing the building height and the street width will have a slightly different effect on cooling ability of the street canyon as a result of the change in the building area fraction.

4.4. *Sensitivity to wind speed*

The idealized case is designed with a low wind speed to simulate favourable conditions for a large UHI effect. In order to quantify the effect of wind speed on the UHI, simulations with different aspect ratios were performed for different wind speeds. Thus these runs differ from the previous simulations as both the wind speed in the initial profile and the geostrophic wind are varied. Runs are presented for geostrophic wind speeds of 6, 10, 15 and 20 m s^{-1}, i.e. higher than the default run with a geostrophic wind speed of 3 m s^{-1}. Figure 5 shows the two different definitions of the UHI for varying wind speed and aspect ratios.

The $\mathrm{UHI}_{\mathrm{max}}$ is not notably sensitive to the aspect ratio as seen in the previous section (Figure 3), but is more sensitive to the wind speed. Changing the wind speed from 3 to 20 m s^{-1} causes $\mathrm{UHI}_{\mathrm{max}}$ to decrease from about 8 to 6 K. The $\mathrm{UHI}_{\mathrm{max}}$ takes place during the start of the evening and the timing stays the same with a higher wind speed; this decrease in the $\mathrm{UHI}_{\mathrm{max}}$ can be explained as follows. An increase in the wind speed enhances the mixing in the surface layer and boundary layer. This enhanced mechanical mixing limits the cooling during the night; as a result the night-time temperatures are enhanced. However, this effect is delayed in the urban simulations compared to the rural simulations. This is because the urban environment is cooling at a slower rate than the rural environment at the time of $\mathrm{UHI}_{\mathrm{max}}$ (section 4.2). Therefore, the urban temperature at this time is similar for different wind speeds and the rural temperature is not. This leads to smaller differences between the rural and urban environment at this time with increased wind speed.

The $\mathrm{UHI}_{T\mathrm{min}}$ reacts similarly to the increased wind speed (Figure 3(a)). The sensitivity of $\mathrm{UHI}_{T\mathrm{min}}$ to the aspect ratio changes only slightly with increased wind speed, from about 3.5 to 8.5 K for 3 m s^{-1} to 1 to 5 K for 20 m s^{-1}. However, comparable to $\mathrm{UHI}_{\mathrm{max}}$, the temperature in the grass simulation increases more than the urban temperature with the wind. Thus, the $\mathrm{UHI}_{T\mathrm{min}}$ decreases with a larger wind speed.

4.5. *Model sensitivity*

In order to test the robustness of the model set-up to its parameter values and to test the sensitivity of the urban canyon temperature to the parameters of the model, 140 simulations were done with the default geostrophic wind of 3 m s^{-1} and an aspect ratio of 1. The model sensitivity of several parameters (road width, roof width, roof height, road and wall albedo, emissivity, thermal conductivity and heat capacity) were explored by doing runs for ten random values for each parameter. These ten values were selected within a realistic range suggested by Loridan *et al.* (2010).

Analysing the results of the various simulations (Figure 6), note that independent of the employed UHI definition, the UHI is not very sensitive to many of the parameters (e.g. the albedo or emissivity). However, the UHI is more sensitive to wall parameters than road parameters, especially to the wall thermal conductivity. Also, the building wall thickness has a clear nonlinear effect on the UHI. This is strongly related to the building's indoor temperature. For thin walls the temperature in the urban canyon is closer to the indoor temperature, whereas thick walls cause the indoor environment to have less influence on the temperature in the urban canyon. In addition, with a wall thickness of 40 cm, the indoor temperature of the building still has a large influence on the UHI. These most sensitive parameters will be taken into account in the next section, when realistic cases are considered.

5. Seasonal dependence

With the understanding gained from the previous section, it is tempting to validate the model findings for realistic cases in Rotterdam. Four representative cases are used with a large UHI

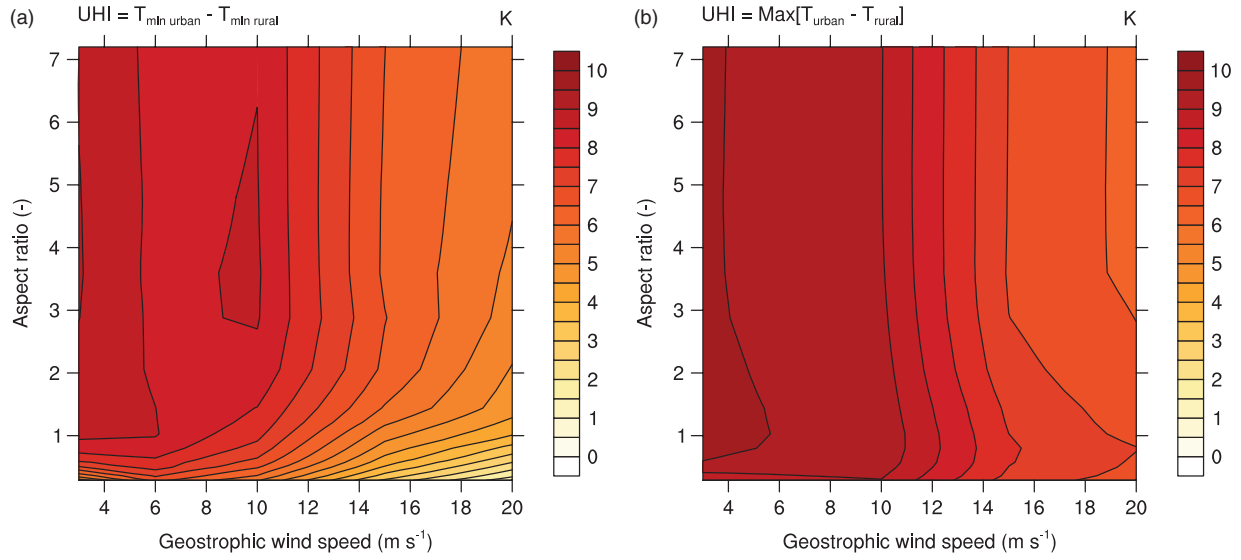

Figure 5. The modelled urban heat island (K), (a) $\mathrm{UHI}_{T\mathrm{min}}$ and (b) $\mathrm{UHI}_{\mathrm{max}}$, for different geostrophic wind speeds and aspect ratios (changing only the width of the street). The model spin-up time is 48 h.

© 2013 Royal Meteorological Society

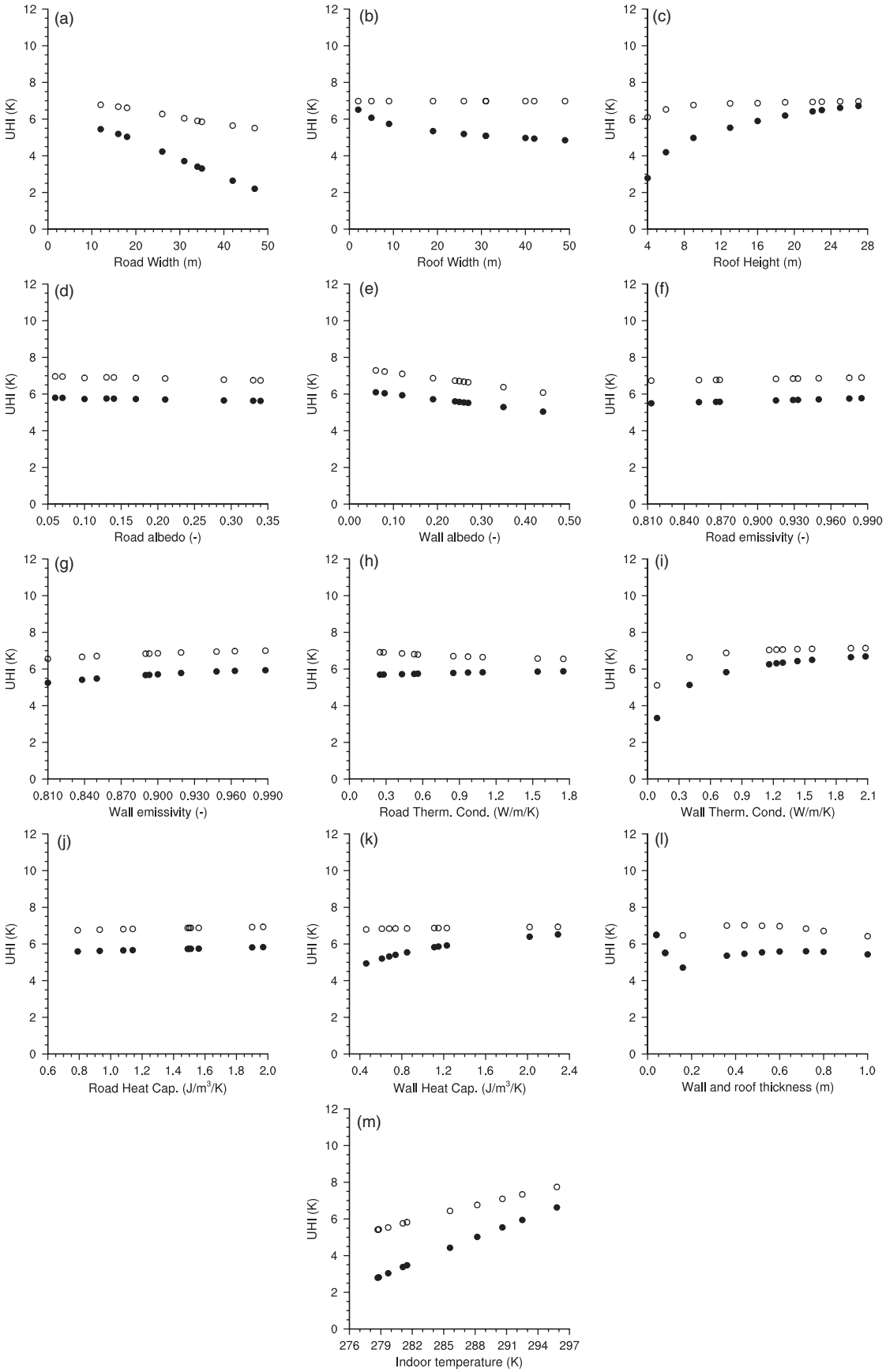

Figure 6. The sensitivity of UHI_{Tmin} (solid circles) and UHI_{max} (open circles) to different parameters in the model: (a) road width, (b) roof width, (c) roof height, albedo of (d) road and (e) wall, emissivity of (f) road and (g) wall, thermal conductivity of (h) road and (i) wall, heat capacity of (j) road and (k) wall, (l) thickness of wall and roof, and (m) indoor temperature. These results are simulated with a geostrophic wind of 3 m s^{-1} and a default aspect ratio of 1. Model spin-up time is 48 h.

potential (e.g. low wind speed, no clouds), one for each season (Table 1). The relation between the UHI and the aspect ratio is evaluated for each case. These results are again compared with observations from different measurement sites with a variety of aspect ratios, as described in Table 2.

5.1. *Case set-up*

Table 1 summarizes the meteorological conditions of the four cases, each representing a season. In addition, a fifth (summer) case is added to compare model results with mobile observations

© 2013 Royal Meteorological Society

Table 1. List of cases and their properties, the prescribed geostrophic wind (U_G), minimum and maximum temperature from observations at Cabauw and the prescribed volumetric soil moisture content (ρ).

Case	U_G ($m\,s^{-1}$)	T_{min} (°C)	T_{max} (°C)	ρ ($m^3\,m^{-3}$)
'Ideal'	3	7	21	0.39
29 Jan 2011	10	−6	1	0.46
29 Mar 2011	3	−3	14	0.43
19 Jul 2010	4	14	27	0.23
01 Oct 2011	3	11	25	0.23
27 Jun 2011	9	17	30	0.28

(tricycle measurements). All cases consider cloudless days with a relatively low geostrophic wind speed ($<10\,m\,s^{-1}$).

Similar to the simulations of the idealized case, the runs are performed for two different surfaces, grassland and an urban surface. As a default the urban simulations use the adjusted urban parameters (e.g. building height, street width (14 m), roof width (14 m), albedo (0.2), urban fraction(100%)) relevant to the city of Rotterdam (section 4.1).

5.2. Observations

For the model validation we used a rural site and an urban site. The rural site is located at Cabauw (51.971°N, 4.927°E), approximately 30 km northeast from the centre of Rotterdam. The measurement site is well-known in boundary-layer research (van Ulden and Wieringa, 1996; Ronda and Bosveld, 2009). It has a grass vegetation over peat and clay soil and is well watered throughout the year.

Observational data from the urban site Centre are taken as an urban location. The site is part of a network of 14 urban measurement stations in Rotterdam (van Hove *et al.*, 2010, Table 2, Figure 7). All stations measure incoming and outgoing long- and short-wave radiation, surface and air temperatures, wind speed and direction, relative humidity and precipitation. Observations from other urban stations are used to assess the relationship between the UHI and aspect ratio. A more detailed description is given in Table 2 and, following the nine requirements of Stewart (2011), we can add:

- Conceptual model: all stations measure within the urban canopy layer; the measuring height varies (Table 2).
- Operational definitions: for each site a UHI is calculated using the same reference station. For this we use the screen-level temperature for all sites.
- Instrument specifications: all stations are standard Campbell (CS215) weather stations with added four-component radiation sensor (Hukseflux NR01) and Black Globe temperature sensor (Sensor Data). Accuracies are: temperature ±0.3 K at 25 °C, ±0.4 K over +5–40 °C; humidity ±2% over 10–90%, ±4% over 0–100%.
- Site metadata: a detailed overview of the site metadata is given in Table 2 and Figure 7 shows the station locations.
- Site representativeness: instruments were placed in representative locations for their local climate zones (Table 2).
- Number of replicates: for each site we only have one temperature measurement.
- Weather control: data for only selected days were used. These cases were selected to be cloudless and with low 10 m wind speeds ($<5\,m\,s^{-1}$ at the reference station).
- Surface control: the city of Rotterdam has a flat surface, with the river Nieuwe Maas running through the city. However we used only stations that have less than 10% water within a radius of 250 m from the station; this was estimated using satellite images.
- Synchronicity: all stations use 30 min averaged quantities.

Despite the fact that the observations fulfil many requirements, it is important to note that the measurement of the urban canyon temperature is not necessarily the average temperature of the street canyon. As recently shown by Park *et al.* (2012), the spatial patterns of heating within an urban canyon greatly depend on street orientation and wind direction. In addition to the stationary observations, traverse measurements are used. These measurements are performed using two cargo tricycles, cycling two routes in and around Rotterdam within the urban canopy layer at several times during the day. The trike measurements are described in detail in Heusinkveld *et al.* (2013). The trikes were equipped with a shielded and ventilated (43502-L Compact Aspirated Shield from R. M. Young, USA) thermometer and humidity sensors (CS215), a 2D ultrasonic anemometer from Solent Windsonic and twelve radiation sensors measuring long- and short-wave radiation in six directions (Hukseflux NR01), all measured and recorded with a Campbell CR1000 data logger, at an interval of 1 s. The measured wind speed is corrected for the trike speed. The measurements were taken on 27 June 2011 between 1900 and 0300 LT (1800 and 0200 UTC), a warm, cloudless day. However, to derive the UHI in the evening, only the measurements between 2000 and 0100 LT are used in our analysis and compared to the reference station of Rotterdam described in Table 2. This day was a cloudless day, but after 0100 LT high cirrus clouds drifted in. During the day the temperature at Rotterdam Airport reached 31.5 °C. Here, only the role of the aspect ratio is analysed. Therefore, only streets with a similar (and low) green fraction are selected, with an aspect ratio ranging between 0.3 and 3.1.

5.3. Case validations

In this section the model spin-up is shorter than in section 4 as the simulations are initialised on the day of interest and no external forcing is applied for simplicity.

In addition, an uncertainty range of the simulations is introduced to provide insights into the sensitivity of the input parameters and the time in the simulation. As was shown in section 4.5, the UHI is sensitive to certain parameters, including the indoor temperature, wall thickness and thermal conductivity. The default values of these parameters were not realistic of the Rotterdam urban area, and a better area-specific estimation

Table 2. Urban weather stations with measuring height (MH), measurement period and the urban and local climate zones (UCZ and LCZ; Oke, 2004; Stewart and Oke, 2012, respectively).

Station name	MH (m)	Period (to present)	UCZ (LCZ)	Aspect ratio	Veg. frac.(%)	Water frac.(%)	Latitude (°N)	Longitude (°E)
Reference station	1.5	28 Aug 2009	Grassland	0.0	90	3	51.986090	4.435750
Groothandelsmarkt	3	21 Jun 2010	4 (extensive lowrise)	0.34	2	2	51.933285	4.415082
Vlaardingen	1.5	22 Jun 2010	3/7 (compact lowrise /sparsely built)	0.449	42	8	51.910967	4.348826
Centre	6	28 Aug 2009	2 (compact midrise)	1.062	2	0	51.922890	4.468070
South	1.5	28 Aug 2009	2 (compact midrise)	0.916	14	0	51.887810	4.487700

The aspect ratio and area-averaged percentage of vegetation and water are within a radius of 250 m of the station.

© 2013 Royal Meteorological Society

Figure 7. The positions of all the measurement stations in the metropolitan area of Rotterdam (source: Google Earth).

of the parameters was made. In order to quantify the model uncertainty, the urban simulations have been repeated for a realistic range. First, the range of the indoor temperature was between 15 and 23 °C, with a default at 17 °C as an average between buildings with climate control on and off. However, in some cases (19 July, 1 October and 27 June) the temperature at the Centre station did not drop below 15 °C and a minimum of 17 °C was used. The thermal conductivity and the thickness of the walls were changed simultaneously, because they both depend on the materials used. As a default, a wall thickness of 0.3 m and thermal conductivity of 1.01 $W m^{-1}K^{-1}$ were used, based on the materials (reinforced concrete and glass windows) of the building next to the weather station. Based on the surrounding buildings, the range was set between an average wall thickness of 0.22 m with an average thermal conductivity of 0.74 $W m^{-1}K^{-1}$ and an average wall thickness of 0.46 m with an average thermal conductivity of 1.68 $W m^{-1}K^{-1}$. The uncertainty range in Figures 8, 9 and 10 indicates the minimum and maximum urban canyon temperature or UHI from the simulations with the described range of parameters (indoor temperature, wall thickness and thermal conductivity). Naturally, the uncertainty of the air temperature at the rural site to surface parameters should also be calculated. However, the difference in 2 m temperature is negligible compared to the uncertainty in the urban simulations.

The winter case of 29 January 2011 is the most challenging of the four cases to be represented by WRF (Figure 8(a)). After the examination of several similar cloudless winter cases (only one shown here), it appears that the model underestimates the night-time temperature and overestimates the daytime temperature in the grassland environment. In this case there is a thin layer of relatively warm and moist air close to the surface. During the night, another layer of moist air appears 2 km above that layer. This layer is not created by the model, as this could be due to advection or subsidence. As soon as the model switches from an unstable to a stable boundary layer, the temperature decreases dramatically. Because of the absence of this moist layer above the boundary layer, the downwelling long-wave radiation is largely underestimated (more than 20 $W m^{-2}$), leading to more cooling close to the surface. The misrepresentation of the stable boundary layer in the winter is a well-known problem of numerical models (Hanna and Yang, 2001; Svensson *et al.*, 2011; Atlaskin and Vihma, 2012). The misrepresentation of the stable boundary layer results in an overestimation of the diurnal temperature range (DTR): since ∼11 K is modelled and ∼6 K measured. The opposite is true for the urban simulation. After initialisation, the modelled temperature is too high for the remainder of the night and the daytime. After 1700 LT the modelled temperature does not fall as much as is seen in the observations. Consequently, the urban DTR is modelled to be only 3 K, while a DTR of 5 K was observed. However, as the simulation progresses, the urban canyon temperature becomes more sensitive to building materials or indoor temperatures. It is assumed that the indoor temperatures do not reach below 15 °C, although during the winter, if buildings are not used, the indoor temperature may be lower, closer to the outdoor temperature. In addition, in reality the indoor temperature may not have a large effect on the canyon temperature, due to e.g. better isolation. The too-high urban night-time temperature and especially the underestimation of the night-time rural temperature (Table 3) results in an UHI overestimation of ∼6 K. During the day, the temperature, especially in the urban environment, is represented well enough by the model for the purpose of our study.

For the spring case on 29 March 2011, the model performs satisfactorily for the 2 m temperature in both the urban and the rural environment (Figure 8(b)). However, similar to the January case, the largest uncertainty in the urban canyon temperature, due to the uncertainty in the model parameters, is seen at night, especially the second night. The UHI is slightly overestimated by the model, because it overestimates the night-time urban canyon temperature and the minimum temperature occurs earlier in the rural observations, amounting to a maximum of 3 K difference.

For the summer case of 19 July 2010, the model has a relatively good representation (Figure 8(c)). However, the 2 m temperature of the grassland simulation is 1–2 K too low. After initialisation at 0000 UTC, the urban area cools too much. This also results in a lower daytime temperature than observed. However, in the evening the model does not cool as fast as measured at this station and the modelled urban temperature meets the observations again. As soon as the sun rises, the modelled canyon air warms faster than the canyon air in the observations. This is the result of the passing of a front, which is not taken into account in the model. Therefore the root mean squared error is also very large in this case (Table 3). Contrary to the other cases, the temperature in the canyon is not very sensitive to the model parameters.

For the autumn case on 1 October 2011, the underestimation of the 2 m temperature in the rural area appears again, but it

© 2013 Royal Meteorological Society

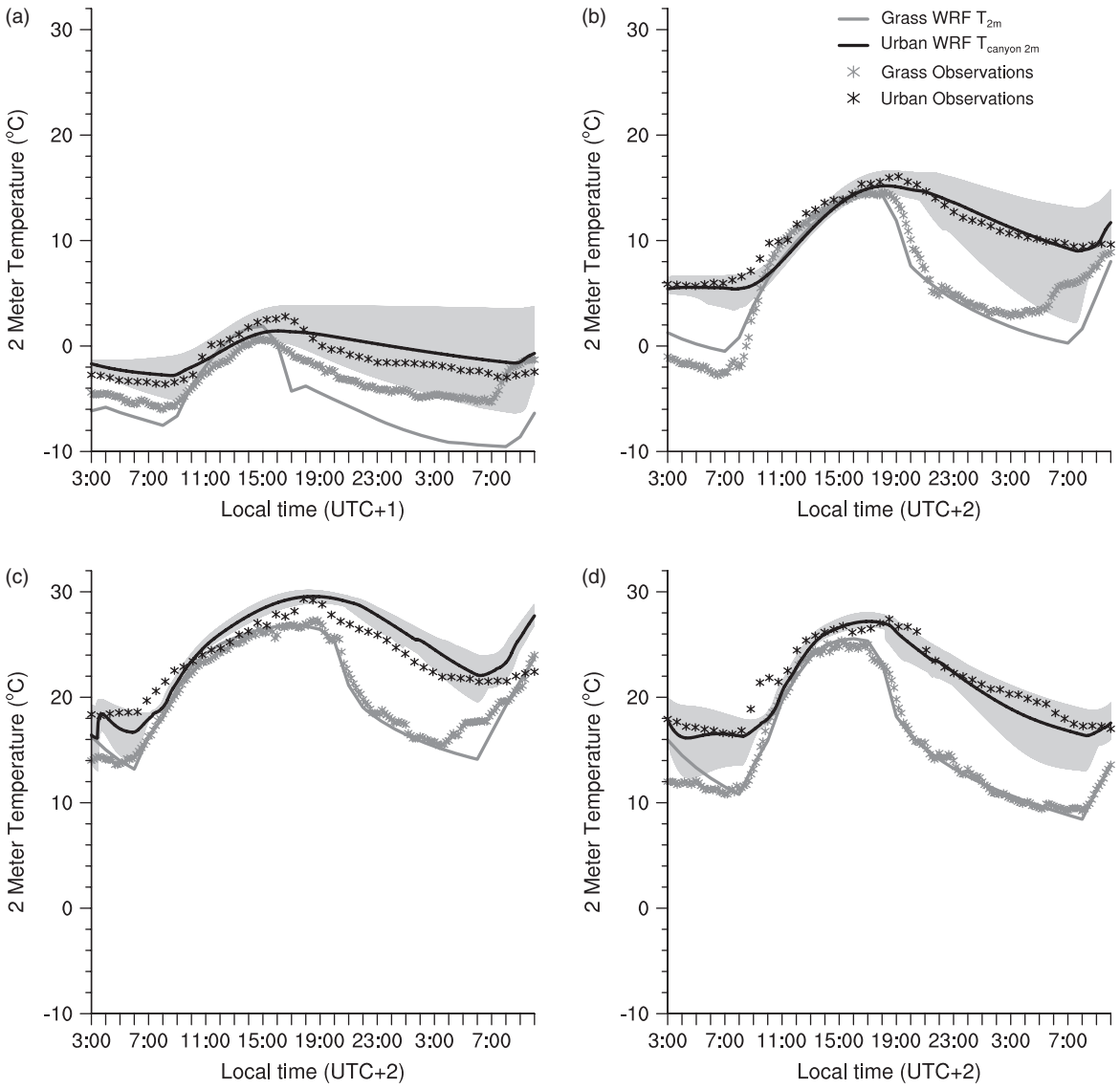

Figure 8. The 2 m temperature from the second hour of the simulation, for four cases on (a) 29 January 2011, (b) 29 March 2011, (c) 19 July 2010 and (d) 1 October 2011, from WRF (lines) and measurements (dots). The grass simulations are compared to measurements at Cabauw, the Netherlands, and the urban simulations to Centre station in the metropolitan area of Rotterdam. The grey areas show the range between the minimum and maximum 2 m canyon temperature from sensitivity simulations (explained in the text, section 5.3). The model spin-up is 1 h.

Table 3. The root mean squared error (°C) of the model output temperature between 0300 LT on the first day and 1000 LT on the second day of the simulation, and the mean bias (°C) of the night-time temperature between 1500 LT and 0800 LT on the second day of the simulation.

	January	March	July	October	Mean
Rural					
RMSE	3.19	2.12	1.13	1.06	1.76
Bias	−3.13	−1.55	−0.81	−0.18	−1.42
Urban					
RMSE	1.38	1.43	2.71	1.38	2.07
Bias	1.39	0.83	2.38	1.01	1.40

has slightly improved compared to the July case (Figure 8d). The urban simulation compares very well with the measurements and is especially sensitive to model parameters during the late night.

Overall, the model performs surprisingly well in simulating the four cases without any external forcing and taking into account the uncertainty of the measurements. The uncertainty range in the model is especially large in the January and March cases due to the large difference between the indoor and outdoor temperatures. The inaccuracies in the model lead to differences in the UHI between the model and observations. For the different cases this amounts to about 6 K for the winter case, 3 K for the spring case, almost no difference for the summer case and less than 1 K in the autumn case.

5.4. *UHI and the aspect ratio*

The modelled UHI as a function of aspect ratio from the idealized case described in section 4.3 is repeated using the four realistic cases. Figure 9 shows the UHI for different aspect ratios in each of the four cases and the uncertainty range of the UHI based on the uncertainty in model parameters.

In the January case the incoming short-wave radiation is limited. Hence trapping of long-wave radiation dominates the relation between the UHI and aspect ratio. This is reflected in the model simulation results in Figure 9(a). Comparing the model results to observations, the model overestimates UHI by ∼6 K. However, if the bias is corrected, the model results are close to the observations, since the shape of the UHI–aspect ratio relation is the simular.

The set-up for the March case is approximately similar to the idealized case in section 4.2 (Figure 9(b)). The relationship between the UHI and aspect ratio is also very similar to the idealized case. The UHI_{max} is less sensitive to the change in aspect ratio than UHI_{Tmin}. The UHI_{max} is reached directly after sunset. Therefore it is sensitive to the lack of solar radiation reaching into the urban canyon during the day for high aspect ratios.

© 2013 Royal Meteorological Society

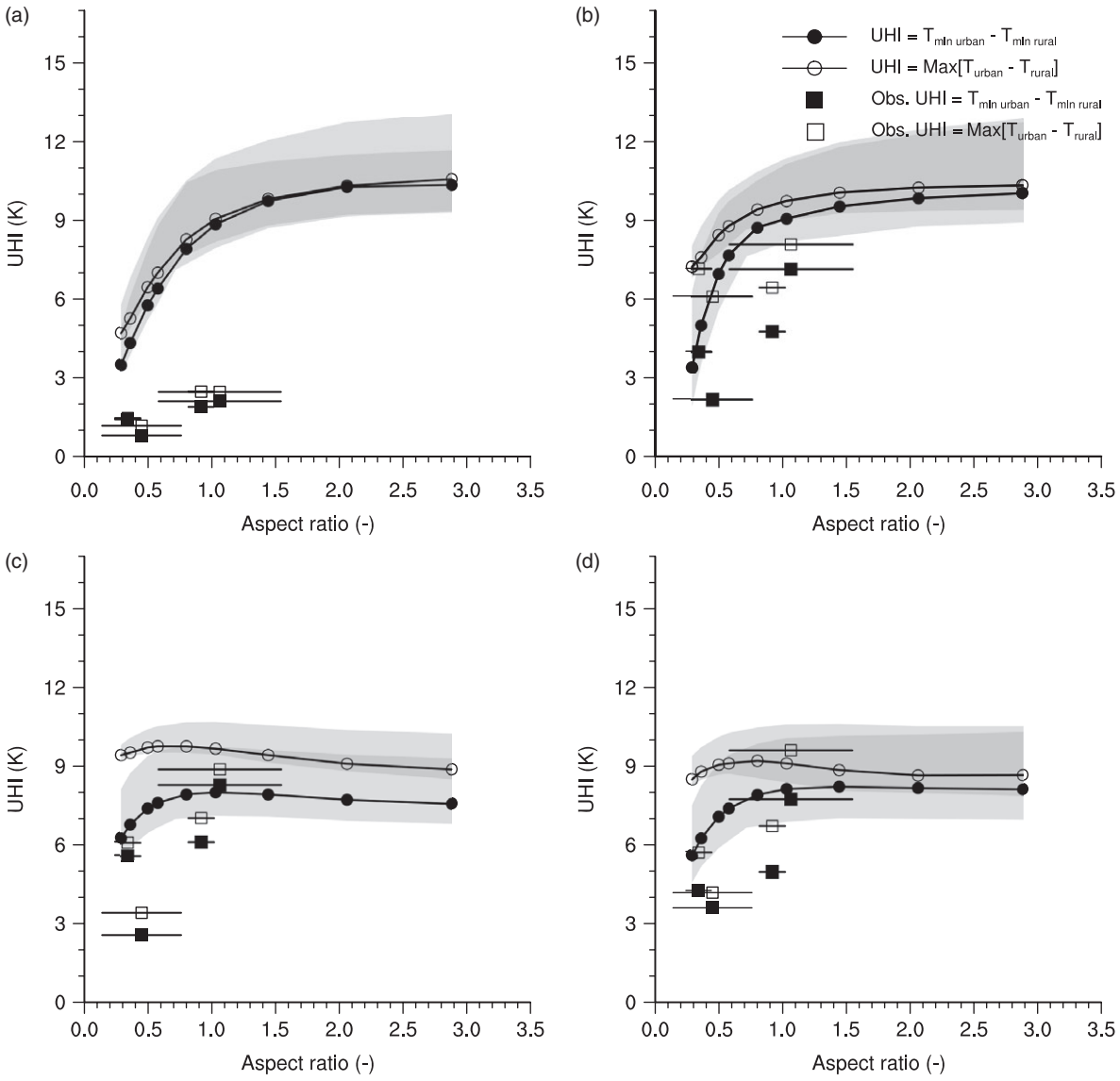

Figure 9. The modelled urban heat island (circles with lines) for different aspect ratios with observations (squares): (a) January, (b) March, (c) July, and (d) October. The grey areas show the range between the minimum and maximum UHI from sensitivity simulations (explained in the text, section 5.3). The model spin-up is 12 h. The UHI is computed within the first full night.

Consequently, the UHI_{max} does not increase much when the aspect ratio is larger than 1. However, the minimum temperature is reached at the end of the night when the trapping of long-wave radiation is controlling the UHI_{Tmin}–aspect ratio relationship. The behaviour of the observations closely resembles the model results. However, as seen in section 5.3, the UHI in the model is overestimated by 3 K, but the shadowing effects are not visible in the UHI_{max}. Unfortunately our observations do not cover aspect ratios larger than 1, where the shadowing effects start to become important.

In the July case trapping of long-wave radiation appears not to be the controlling factor in the relationship between the aspect ratio and UHI (Figure 9(c)). Only when the aspect ratio is below 0.5 does it have an enhanced effect on the UHI. Adopting a larger aspect ratio leads to a decreasing UHI; shadowing effects become important, both for the early and the late night. In July, midlatitude nights are short and days are long. Therefore, the solar radiation input is relatively high in this season and plays a more important role than trapping of long-wave radiation in the contribution of the aspect ratio to the UHI. The observations in the July case do not support the modelled results. The observations show a positive relation between the aspect ratio and the UHI, whereas a negative relation found using the model. An explanation may be that the observations were influenced by other factors, such as a difference in vegetation, anthropogenic heat, building materials, etc. In addition, the range of observed aspect ratios is very small. Shadowing effects may also start to be important for larger aspect ratios (>3), as shown by Marciotto *et al.* (2010). However, section 5.5 will show that the shadowing effects can play a role in the relation between the UHI and the aspect ratio of the street canyon.

Close to the equinox as in the March and the idealized cases, the October case has a similar relation between the street geometry and the UHI (Figure 9(d)). However, the influence of the aspect ratio on the UHI_{max}, in the early night, is mostly dependent on the shadowing effects and the UHI_{max} slightly decreases with the aspect ratio. The UHI_{Tmin}, in the late night, is mostly influenced by the trapping of long-wave radiation, particularly with an aspect ratio lower than 1. For higher values of the aspect ratio, UHI_{Tmin} remains constant when the aspect ratio increases. The observed relation is similar to the modelled relation for UHI_{Tmin}; the UHI increases with the aspect ratio. However, the observations do not reach further than an aspect ratio of 1 and it is unknown if the UHI remains constant for higher aspect ratios.

The uncertainty of the UHI is in the order of 1 or 2 K and larger at the time of UHI_{Tmin}, due to the accumulation of uncertainties. Most importantly, changing the model parameters does not change the shape of the relationship between the UHI and aspect ratio; only the value of the UHI changes.

© 2013 Royal Meteorological Society

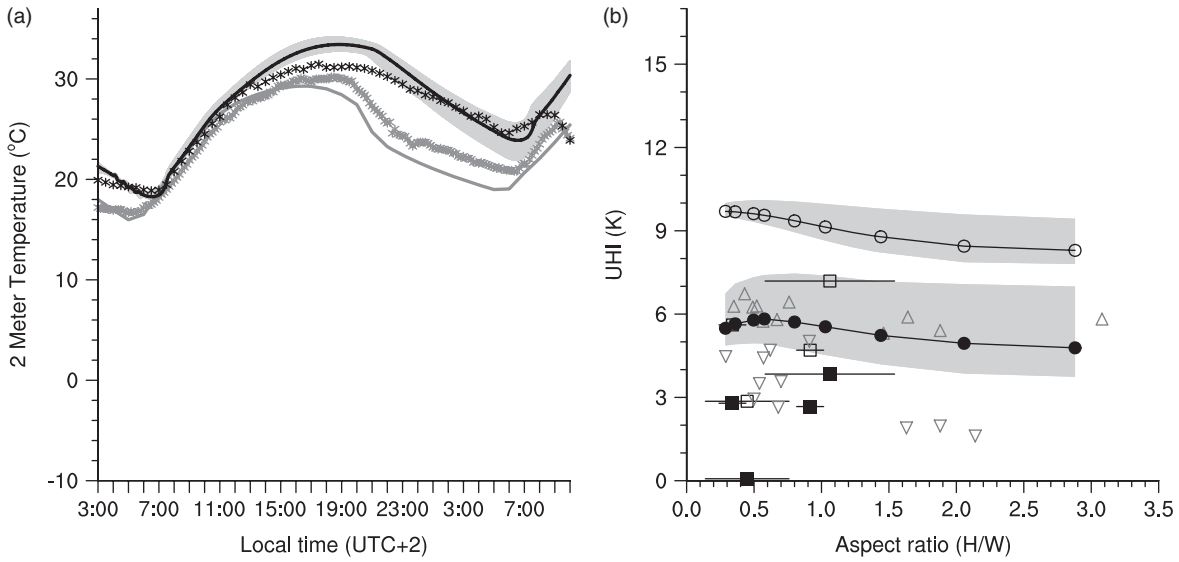

Figure 10. (a) As Figure 8 (RMSE: urban 1.18 °C, rural 1.48 °C), and (b) as Figure 9, but for the case of 27 June 2011. (b) shows additional observations from the tricycle traverse measurement (grey), split between observations taken within a 2000 m radius of the centre of the city (up-pointing triangles) and outside this radius (down-pointing triangles).

5.5. *Comparison with traverse measurements*

In section 5.4 the stationary weather stations could not completely confirm the modelled relation between the aspect ratio and the UHI. The measurements of the station confirmed the effect of trapping of long-wave radiation. However, the shadowing effects were less visible. In order to test whether this is due to the different environments of the weather stations (different green fraction, anthropogenic heat, building materials, etc.), mobile measurements were used. Since UHI cases with these measurements are rare, an additional case with available trike traverse observations was set up. During this case the wind was relatively high (10 m wind speed outside the city reached up to 5 m s^{-1}).

An effect of advection can be seen in the temperatures in Figure 10(a). The model simulations are close to the observations after initialisation. However, in the afternoon the city is cooler than modelled and does not cool down as much during the night. In the rural area the main difference in the modelled and observed temperature is during the evening and night. In the model the rural environment cools down much earlier and more than in reality. The fact that both runs are cooler by the end of the night still gives smaller error in $\mathrm{UHI}_{T\mathrm{min}}$ (Figure 10(b)). However, the cooling rates in both the rural and urban simulations are incorrect and this leads to a large overestimation of the $\mathrm{UHI}_{\mathrm{max}}$.

In Figure 10(b) the model results show the relationship between the UHI and aspect ratio is mostly negative as in Figure 9(c). This means that shadowing effects are dominant in this case. The available short-wave radiation at this time is even larger than in the July case, because the timing is closer to the summer solstice. As in section 5.4, the stationary weather stations do not confirm the shadowing effect on the UHI–aspect ratio relationship. This may be due to the fact that the range of aspect ratios is small. Results of Marciotto *et al.* (2010) indicate that shadowing effects may become important at an aspect ratio larger than 3.5. In this study, the shadowing effect was also found to have an impact on the UHI–aspect ratio relation, starting at an aspect ratio between 0.5 and 1.

The tricycle measurements do confirm the shadowing effect on the UHI, both inside and outside the city centre; streets located outside the centre of the city especially show a decreasing UHI with increased aspect ratio. The mobile observations within the centre do not show a large negative change in UHI with increasing aspect ratio. However, this neither confirms the short-wave shadow nor rules out the trapping of long-wave radiation effects. The UHI values of the tricycle measurements are lower than the model $\mathrm{UHI}_{\mathrm{max}}$ as a result of the model bias. In addition, the observations outside the city centre are influenced by local advection from outside the city and have lower UHI values than the observations in the city centre.

This large difference in the results found with stationary and mobile measurements indicates that care should be taken in the placing of the instruments (i.e. inside the urban canyon, similar vegetation fraction, building properties, etc.).

Overall, this modelling approach appears to be to useful in understanding the mechanisms involved in the UHI–aspect ratio relationship. Depending on the case, the one-dimensional model simulations are able to reproduce the UHI. However, in cases where advection is an important contributor, this modelling approach has more difficulties in reproducing the measured temperature. For example, the January case was not well reproduced by the model, possibly due to this lack of advection. Here a three-dimensional model might give better results.

The definition of this UHI with the mobile measurements is slightly different from the other observations. Since the measurements were taken during the start of the night they should be compared to $\mathrm{UHI}_{\mathrm{max}}$, which is overestimated by the model.

Using the mobile tricycle measurements we are able confirm that, besides the trapping of long-wave radiation effect shown by the stationary weather stations, the shadowing effects also play an important role in the relation between the street canyon aspect ratio and the UHI.

6. Conclusions

In this article the different processes involved in determining the effect of the aspect ratio on the UHI are analysed. This is done using a novel modelling technique –a single-column model employed with an urban canopy model, and the results are evaluated using observations. In doing so, this study shows that the relation between the aspect ratio and the UHI is more complex than previously thought. We were able to reproduce and understand the results of Marciotto *et al.* (2010) with a different urban canopy model than the one used by them.

We found that the UHI is controlled by two counteracting processes. First, by the process of trapping of long-wave radiation, which has an increased effect on the UHI. It causes more long-wave radiation to be trapped when buildings are higher and streets are more narrow. Secondly, the process of shadowing has a decreased effect on the UHI within the urban canopy. As streets

© 2013 Royal Meteorological Society

narrow, less solar radiation reaches into the canyon, leading to less heating during the day. This causes the night-time temperature and thus the UHI to stabilise and in some cases even decrease when streets become more narrow. This adds to the findings by Oke (1981, 1988), using only one maximum UHI throughout the year to find a positive relation between the UHI and aspect ratio.

We were able to confirm these two processes with two different kinds of observations. Firstly, the effect of trapping of long-wave radiation was confirmed by the stationary weather stations located in different urban areas. Secondly, the shadowing effects were observed in a summer case with mobile traverse measurements.

Which of these two processes dominates the effect of street geometry on the UHI depends on many factors. Most important are the time during the night at which the UHI takes place (depending on the definition of the UHI) and the overall available short-wave radiation (depending on the season, latitude, cloudiness, etc.). At the start of the night the shadowing effects play an important role, while later during the night the trapping of long-wave radiation regulates the effect on the UHI. The individual processes influencing the available short-wave radiation should be the subject of further study.

Acknowledgements

This study was sponsored by the NWO Sustainable Accessibility to the Randstad. We thank the municipality of Rotterdam for providing the datasets of the monitoring network, Jan Elbers (Alterra) for pre-processing the observational data, and Fred Bosveld (Royal Netherlands Meteorological Institute) for the observations from Cabauw. Leo Kroon is thanked for his useful suggestions on the manuscript. Bert Heusinkveld and Reinder Ronda would also like to thank the Climate-Proof Cities project from Knowledge for Climate.

Appendix

Extended model description

The wind speed at roof level is described by (Loridan *et al.*, 2010)

$$U_{\mathrm{R}} = U_{\mathrm{A}} \frac{\ln\left(\frac{Z_{\mathrm{R}}-Z_{\mathrm{D}}}{Z_{0\mathrm{C}}}\right)}{\ln\left(\frac{Z_{\mathrm{A}}-Z_{\mathrm{D}}}{Z_{0\mathrm{C}}}\right)}.$$

Here U_{A} is the wind speed at the lowest model level, Z_{R} the roof level height, Z_{D} the displacement height (1/5 of the roof level height), $Z_{0\mathrm{C}}$ is the roughness length for momentum above the canyon (10% of the roof level height) and Z_{A} is the height of the first atmospheric model level. From the wind speed at roof level, the wind speed in the canyon is calculated as (Loridan *et al.*, 2010)

$$U_{\mathrm{C}} = U_{\mathrm{R}} \exp\left\{-a\left(1-\frac{Z_{\mathrm{C}}}{Z_{\mathrm{R}}}\right)\right\}.$$

In this case, a is the attenuation constant (Inoue, 1963) and Z_{C} is the height at which the wind speed is calculated in the canyon ($0.7Z_{\mathrm{R}}$).

When examining the street canyon geometry, it is important to have a good representation of short- and long-wave radiation in the model. The short-wave radiation that reaches the roof (S_{R}), walls (S_{W1} and S_{W2}) and the road (S_{G1} and S_{G2}) is given by Kusaka *et al.* (2001):

$$\begin{aligned}
S_{\mathrm{R}} &= S_{\mathrm{X}}(1-\alpha_{\mathrm{R}}),\\
S_{\mathrm{W1}} &= S_{\mathrm{X}} F_{\mathrm{W}\to\mathrm{S}}(1-\alpha_{\mathrm{W}}),\\
S_{\mathrm{W2}} &= S_{\mathrm{G1}} \frac{\alpha_{\mathrm{G}}}{1-\alpha_{\mathrm{G}}} F_{\mathrm{W}\to\mathrm{G}}(1-\alpha_{\mathrm{W}}),\\
S_{\mathrm{G1}} &= S_{\mathrm{X}} F_{\mathrm{G}\to\mathrm{S}}(1-\alpha_{\mathrm{G}}),\\
S_{\mathrm{G2}} &= S_{\mathrm{W1}} \frac{\alpha_{\mathrm{W}}}{1-\alpha_{\mathrm{W}}} F_{\mathrm{G}\to\mathrm{W}}(1-\alpha_{\mathrm{G}}),
\end{aligned}$$

where S_{X} is the solar radiation received by the horizontal surfaces. The albedo of the roof, walls and road is given by α_{R}, α_{W} and α_{G}, respectively. $F_{\mathrm{W}\to\mathrm{S}}$ is the sky-view factor integrated over the wall (Sakakibara, 1996). Similarly, $F_{\mathrm{W}\to\mathrm{W}}$ is the wall-view factor of a wall, $F_{\mathrm{W}\to\mathrm{G}}$ the road-view factor integrated over the wall, $F_{\mathrm{G}\to\mathrm{S}}$ the sky-view factor of the road, and $F_{\mathrm{G}\to\mathrm{W}}$ the wall-view factor integrated over the ground.

As for the long-wave radiation, a similar method is used:

$$\begin{aligned}
L_{\mathrm{R}} &= \epsilon_{\mathrm{R}}\left(L^{\downarrow} - \sigma\, T_{\mathrm{R}}^4\right),\\
L_{\mathrm{W1}} &= \epsilon_{\mathrm{W}}\left(L^{\downarrow} F_{\mathrm{W}\to\mathrm{S}} + \epsilon_{\mathrm{G}}\,\sigma\, T_{\mathrm{G}}^4 F_{\mathrm{W}\to\mathrm{G}}\right.\\
&\qquad \left. + \epsilon_{\mathrm{W}}\,\sigma\, T_{\mathrm{W}}^4 F_{\mathrm{W}\to\mathrm{W}} - \sigma\, T_{\mathrm{W}}^4\right),\\
L_{\mathrm{W2}} &= \epsilon_{\mathrm{W}}\Big\{(1-\epsilon_{\mathrm{G}}) L^{\downarrow} F_{\mathrm{G}\to\mathrm{S}} F_{\mathrm{W}\to\mathrm{G}}\\
&\qquad + (1-\epsilon_{\mathrm{G}})\,\epsilon_{\mathrm{W}}\,\sigma\, T_{\mathrm{W}}^4 F_{\mathrm{G}\to\mathrm{W}} F_{\mathrm{W}\to\mathrm{G}}\\
&\qquad + (1-\epsilon_{\mathrm{W}})\, L^{\downarrow} F_{\mathrm{W}\to\mathrm{S}} F_{\mathrm{W}\to\mathrm{W}}\\
&\qquad + (1-\epsilon_{\mathrm{W}})\,\epsilon_{\mathrm{G}}\,\sigma\, T_{\mathrm{G}}^4 F_{\mathrm{W}\to\mathrm{G}} F_{\mathrm{W}\to\mathrm{W}}\\
&\qquad + \epsilon_{\mathrm{W}}(1-\epsilon_{\mathrm{W}})\,\sigma\, T_{\mathrm{W}}^4 F_{\mathrm{W}\to\mathrm{W}} F_{\mathrm{W}\to\mathrm{W}}\Big\},\\
L_{\mathrm{G1}} &= \epsilon_{\mathrm{G}}\left(L^{\downarrow} F_{\mathrm{G}\to\mathrm{S}} + \epsilon_{\mathrm{W}}\,\sigma\, T_{\mathrm{W}}^4 F_{\mathrm{G}\to\mathrm{W}} - \sigma\, T_{\mathrm{G}}^4\right),\\
L_{\mathrm{G2}} &= \epsilon_{\mathrm{G}}\Big\{(1-\epsilon_{\mathrm{W}}) L^{\downarrow} F_{\mathrm{W}\to\mathrm{S}} F_{\mathrm{G}\to\mathrm{W}}\\
&\qquad + (1-\epsilon_{\mathrm{W}})\epsilon_{\mathrm{G}}\,\sigma\, T_{\mathrm{G}}^4 F_{\mathrm{W}\to\mathrm{G}} F_{\mathrm{G}\to\mathrm{W}}\\
&\qquad + \epsilon_{\mathrm{W}}(1-\epsilon_{\mathrm{W}})\,\sigma\, T_{\mathrm{W}}^4 F_{\mathrm{W}\to\mathrm{W}} F_{\mathrm{G}\to\mathrm{W}}\Big\},
\end{aligned}$$

where $L^{\downarrow}$ is the downward atmospheric long-wave radiation above the urban canopy, ϵ_{R}, ϵ_{W} and ϵ_{G} are the emissivities of the roof, wall and road and T_{R}, T_{W} and T_{G} are the surface temperatures of the roof, wall and road.

References

Atlaskin E, Vihma T. 2012. Evaluation of NWP results for wintertime nocturnal boundary-layer temperatures over Europe and Finland. *Q. J. R. Meteorol. Soc.* **138**: 1440–1451, doi: 10.1002/qj.1885.

Beljaars ACM, Bosveld FC. 1997. Cabauw data for the validation of land surface parameterization schemes. *J. Clim.* **10**: 1172–1193, doi: 10.1175/1520-0442(1997)0101172:cdftvo2.0.CO;2.

Chen F, Kusaka H, Bornstein R, Ching J, Grimmond CSB, Grossman-Clarke S, Loridan T, Manning KW, Martilli A, Miao S, Sailor D, Salamanca FP, Taha H, Tewari M, Wang X, Wyszogrodzki AA, Zhang C. 2011. The integrated WRF/urban modelling system: Development, evaluation, and applications to urban environmental problems. *Int. J. Climatol.* **31**: 273–288, doi: 10.1002/joc.2158.

Chow WTL, Roth M. 2006. Temporal dynamics of the urban heat island of Singapore. *Int. J. Climatol.* **26**: 2243–2260, doi: 10.1002/joc.1364.

Dudhia J. 1989. Numerical study of convection observed during the winter monsoon experiment using a mesoscale two-dimensional model. *J. Atmos. Sci.* **46**: 3077–3107, doi: 10.1175/1520-0469(1989)0463077:nsocod 2.0.CO;2.

Ek MB, Mitchell KE, Lin Y, Rogers E, Grunmann P, Koren V, Gayno G, Tarpley JD. 2003. Implementation of Noah land surface model advances in the National Centers for Environmental Prediction operational mesoscale Eta model. *J. Geophys. Res.* **108**: D22, doi: 10.1029/2002JD003296.

Fischer EM, Schär C. 2010. Consistent geographical patterns of changes in high-impact European heatwaves. *Nat. Geosci.* **3**: 398–403.

Gallo KP, McNab AL, Karl TR, Brown JF, Hood JJ, Tarpley JD. 1993. The use of a vegetation index for assessment of the urban heat island effect. *Int. J. Remote Sens.* **14**: 2223–2230, doi: 10.1080/01431169308954031.

Giannopoulou K, Santamouris M, Livada I, Georgakis C, Caouris Y. 2010. The impact of canyon geometry on intra-urban and urban: Suburban night temperature differences under warm weather conditions. *Pure Appl. Geophys.* **167**: 1433–1449.

Grimmond CSB, Blackett M, Best M, Barlow J, Baik JJ, Belcher S, Bohnenstengel S, Calmet I, Chen F, Dandou A, Fortuniak K, Gouvea M, Hamdi R, Hendry M, Kawai T, Kawamoto Y, Kondo H, Krayenhoff E, Lee SH, Loridan T, Martilli A, Masson V, Miao S, Oleson K, Pigeon G, Porson A, Ryu YH, Salamanca F, Shashua-Bar L, Steeneveld GJ, Tombrou M, Voogt J, Young D, Zhang N. 2010. The international urban energy balance models comparison project: First results from phase 1. *J. Appl. Meteorol. Climatol.* **49**: 1268–1292.

Grimmond CSB, Blackett M, Best M, Baik JJ, Belcher S, Beringer J, Bohnenstengel S, Calmet I, Chen F, Coutts A, Dandou A, Fortuniak K, Gouvea M, Hamdi R, Hendry M, Kanda M, Kawai T, Kawamoto Y, Kondo H, Krayenhoff E, Lee SH, Loridan T, Martilli AMV, Miao S, Oleson K,

© 2013 Royal Meteorological Society

Ooka R, Pigeon G, Porson A, Ryu YH, Salamanca F, Steeneveld G, Tombrou M, Voogt J, Young D, Zhang N. 2011. Initial results from phase 2 of the international urban energy balance model comparison. *Int. J. Climatol.* **31**: 244–272.

Hamdi R, Schayes G. 2008. Sensitivity study of the urban heat island intensity to urban characteristics. *Int. J. Climatol.* **28**: 973–982, doi: 10.1002/joc.1598.

Hanna SR, Yang R. 2001. Evaluations of mesoscale models' simulations of near-surface winds, temperature gradients, and mixing depths. *J. Appl. Meteorol.* **40**: 1095–1104, doi: 10.1175/1520-0450(2001)0401095:eommso2.0.CO;2.

Harman IN, Belcher SE. 2006. The surface energy balance and boundary layer over urban street canyons. *Q. J. R. Meteorol. Soc.* **132**: 2749–2768, doi: 10.1256/qj.05.185.

Heusinkveld BG, Steeneveld GJ, van Hove LWA, Jacobs CMJ, Holtslag AAM. 2013. Spatial variability of the Rotterdam urban heat island as influenced by urban land use. *J. Geophys. Res.*, doi:10.1002/2012JD019399 (in press).

Hidalgo J, Pigeon G, Masson V. 2008. Urban-breeze circulation during the CAPITOUL experiment: Observational data analysis approach. *Meteorol. Atmos. Phys.* **102**: 223–241.

Högström U. 1996. Review of some basic characteristics of the atmospheric surface layer. *Boundary Layer Meteorol.* **78**: 215–246, doi: 10.1007/BF00120937.

Hong SY, Noh Y, Dudhia J. 2006. A new vertical diffusion package with an explicit treatment of entrainment processes. *Mon. Weather Rev.* **134**: 2318–2341, doi: 10.1175/MWR3199.1.

Houet T, Pigeon G. 2011. Mapping urban climate zones and quantifying climate behaviors –an application on Toulouse urban area (France). *Environ. Pollut.* **159**: 2180–2192, doi: 10.1016/j.envpol.2010.12.027.

van Hove LWA, Steeneveld GJ, Jacobs CMJ, Maat HW, Heusinkveld BG, Moors EJ, Holtslag AAM. 2010. 'Modelling and observing urban climate in the Netherlands'. Technical report. ALTERRA: Wageningen, The Netherlands. http://edepot.wur.nl/173792.

Hu XM, Nielsen-Gammon JW, Zhang F. 2010. Evaluation of three planetary boundary-layer schemes in the WRF Model. *J. Appl. Meteorol. Climatol.* **49**: 1831–1844, doi: 10.1175/2010JAMC2432.1.

Inoue E. 1963. On the turbulent structure of airflow within crop canopies. *J. Meteorol. Soc. Japan.* **41**: 317–326.

Kim YH, Baik JJ. 2005. Spatial and temporal structure of the urban heat island in Seoul. *J. Appl. Meteorol.* **44**: 591–605.

Kovats RS, Hajat S. 2008. Heat stress and public health: A critical review. *Annu. Rev. Public Health* **29**: 41–55, doi: 10.1146/annurev.publhealth.29.020907.090843.

Kusaka H, Kondo H, Kikegawa Y, Kimura F. 2001. A simple single-layer urban canopy model for atmospheric models: Comparison with multi-layer and slab models. *Boundary-Layer Meteorol.* **101**: 329–358.

Lenzhölzer S, Van der Wulp NY. 2010. Thermal experience and perception of the built environment in Dutch urban squares. *J. Urban Des.* **15**: 375–401, doi: 10.1080/13574809.2010.488030.

Lin YL, Farley RD, Orville HD. 1983. Bulk parameterization of the snow field in a cloud model. *J. Clim. Appl. Meteorol.* **22**: 1065–1092, doi: 10.1175/1520-0450(1983)0221065:bpotsf2.0.CO;2.

Loridan T, Grimmond CSB, Grossman-Clarke S, Chen F, Tewari M, Manning K, Martilli A, Kusaka H, Best M. 2010. Trade-offs and responsiveness of the single-layer urban canopy parametrization in WRF: An offline evaluation using the moscem optimization algorithm and field observations. *Q. J. R. Meteorol. Soc.* **136**: 997–1019, doi: 10.1002/qj.614.

Marciotto E, Oliveira A, Hanna S. 2010. Modeling study of the aspect ratio influence on urban canopy energy fluxes with a modified wall-canyon energy budget scheme. *Build. Environ.* **45**: 2497–2505.

Masson V, Grimmond CSB, Oke TR. 2002. Evaluation of the town energy balance (TEB) scheme with direct measurements from dry districts in two cities. *J. Appl. Meteorol.* **41**: 1011–1026.

McCarthy MP, Best MJ, Betts RA. 2010. Climate change in cities due to global warming and urban effects. *Geophys. Res. Lett.* **37**: L09705, doi: 10.1029/2010GL042845.

Mlawer EJ, Taubman SJ, Brown PD, Iacono MJ, Clough SA. 1997. Radiative transfer for inhomogeneous atmospheres: RRTM, a validated correlated-k model for the longwave. *J. Geophys. Res.* **102**: 16663–16682, doi: 10.1029/97JD00237.

Oke TR. 1981. Canyon geometry and the nocturnal urban heat island: Comparison of scale model and field observations. *J. Climatol.* **1**: 237–254.

Oke TR. 1982. The energetic basis of the urban heat island. *Q. J. R. Meteorol. Soc.* **108**: 1–24, doi: 10.1002/qj.49710845502.

Oke TR. 1988. Street design and urban canopy layer climate. *Energy Build.* **11**: 103–113.

Oke TR. 2004. 'Initial guidance to obtain representative meteorological observations at urban sites', IOM report 81. World Meteorological Organization: Geneva, Switzerland.

Oke TR, Johnson G, Steyn D, Watson I. 1991. Simulation of surface urban heat islands under 'ideal' conditions at night, Part 2: Diagnosis of causation. *Boundary-Layer Meteorol.* **56**: 339–358.

Oke TR, Spronken-Smith RA, Jáuregui E, Grimmond CSB. 1999. The energy balance of central Mexico City during the dry season. *Atmos. Environ.* **33**: 3919–3930.

Park SB, Baik JJ, Raasch S, Letzel MO. 2012. A large-eddy simulation study of thermal effects on turbulent flow and dispersion in and above a street canyon. *J. Appl. Meteorol. Climatol.* **51**: 829–841, doi: 10.1175/JAMC-D-11-0180.1.

Pearlmutter D, Berliner P, Shaviv E. 2005. Evaluation of urban surface energy fluxes using an open-air scale model. *J. Appl. Meteorol.* **44**: 532–545, doi: 10.1175/JAM2220.1.

Pino D, de Arellano JVG, Comerón A, Rocadenbosch F. 2004. The boundary layer growth in an urban area. *Sci. Total Environ.* **334–335**: 207–213, doi: 10.1016/j.scitotenv.2004.04.039.

Ronda RJ, Bosveld FC. 2009. Deriving the surface soil heat flux from observed soil temperature and soil heat flux profiles using a variational data assimilation approach. *J. Appl. Meteorol. Climatol.* **48**: 644–656, doi: 10.1175/2008JAMC1930.1.

Sakakibara Y. 1996. A numerical study of the effect of urban geometry upon the surface energy budget. *Atmos. Environ.* **30**: 487–496.

Skamarock W, Klemp J, Dudhia J, Gill D, Barker D, Duda M, Huang XY, Wang W, Powers J. 2008. 'A description of the advanced research WRF version 3', NCAR Technical Note. NCAR: Boulder, CO.

Solomon S, Qin D, Manning M, Chen Z, Marquis M, Averyt K, Tignor M, Miller H. 2007. 'Contribution of working group I to the fourth assessment report of the intergovernmental panel on climate change', IPCC Technical report. Cambridge University Press: Cambridge, UK and New York, NY. http://www.ipcc.ch/publications_and_data/publications_ipcc_fourth_assessment_report_wg1_report_the_physical_science_basis.htm

Steeneveld GJ, Koopmans S, Heusinkveld BG, van Hove LWA, Holtslag AAM. 2011. Quantifying urban heat island effects and human comfort for cities of variable size and urban morphology in the Netherlands. *J. Geophys. Res.* **116**: D20, doi: 10.1029/2011JD015988.

Stewart ID. 2011. A systematic review and scientific critique of methodology in modern urban heat island literature. *Int. J. Climatol.* **31**: 200–217, doi: 10.1002/joc.2141.

Stewart ID, Oke TR. 2012. 'Local climate zones' for urban temperature studies. *Bull. Am. Meteorol. Soc.* **93**: 1879–1900, doi: 10.1175/BAMS-D-11-00019.1.

Svensson G, Holtslag A, Kumar V, Mauritsen T, Steeneveld G, Angevine W, Bazile E, Beljaars A, Bruijn E, Cheng A, Conangla L, Cuxart J, Ek M, Falk M, Freedman F, Kitagawa H, Larson V, Lock A, Mailhot J, Masson V, Park S, Pleim J, Söderberg S, Weng W, Zampieri M. 2011. Evaluation of the diurnal cycle in the atmospheric boundary layer over land as represented by a variety of single-column models: The second GABLS experiment. *Boundary Layer Meteorol.* **140**: 177–206, doi: 10.1007/s10546-011-9611-7.

United Nations. 2006. 'The 2004 revision and world urbanisation prospects: The 2005 revision'.

van Ulden AP, Wieringa J. 1996. Atmospheric boundary layer research at Cabauw. *Boundary Layer Meteorol.* **78**: 39–69, doi: 10.1007/BF00122486.

© 2013 Royal Meteorological Society